Target-state dependence of cross sections for reactions on statically deformed nuclei

F. S. Dietrich, I. J. Thompson, and T. Kawano

Target-state dependence of cross sections for reactions on statically deformed nuclei

F. S. Dietrich* and I. J. Thompson

Lawrence Livermore National Laboratory, Livermore, CA 94550

T. Kawano

Los Alamos National Laboratory, Los Alamos, NM 87545

As part of an effort to understand how neutron-induced reactions on excited states in deformed nuclei differ from those on ground states, we have carried out coupled-channels calculations of the angle-integrated cross sections on the ground and excited states of several actinide nuclei with differing K-values for the ground-state band (^{233}U, $K = \frac{5}{2}$; ^{235}U, $K = \frac{7}{2}$; ^{238}U, $K = 0$; and ^{239}Pu, $K = \frac{1}{2}$). Of particular interest is the compound-nucleus formation cross section. We find that the ratio of the excited to ground-state compound formation cross sections is very close to unity in all cases (within $\approx 0.1\%$) over the range studied (1 keV to 20 MeV). This result requires that sufficient levels be coupled to ensure convergence (approximately 14 levels for odd-A nuclei). These results are close to the predictions of the adiabatic model for scattering from statically deformed nuclei. This model yields compound formation cross sections, as well as total cross sections, that are independent of both the K-value of the band and the spin of the target state within the band. Our calculations show that the actual cross sections are surprisingly close to the adiabatic limit, even at very low incident energies. We find similar results for statically deformed rare-earth and s-d shell nuclei.

PACS numbers: 24.10.Eq, 24.10.Ht, 25.40.-h, 28.20.Cz, 28.20.Fc

I. INTRODUCTION

In many applications we want the cross sections for the production of compound-nucleus (CN) states when neutrons are incident on rotational nuclei. This cross section, also known as the fusion or absorption cross section, is needed for rotational nuclei which are particularly common in the rare earth and actinide regions. In some hot astrophysical environments we also need the equivalent cross sections for nuclei in initial excited states.

It is well known that coupled-channels calculations are needed for these reactions, and the recent paper of Kawano *et al.* [1] reported on such calculations where five levels of ^{169}Tm were included to calculate the compound-nucleus cross section for neutrons incident on both the ground and first-excited states. They also studied the target-state dependence of the ^{239}Pu fission cross section. The results of that paper were an important stimulus for the present work, in which we have made a systematic study of the behavior of the excited *vs.* ground-state cross sections in statically deformed nuclei in three regions of the periodic table, including an investigation of the dependence of the cross sections on the number of states included in the coupled-channels calculations.

In the course of the present research it became apparent that the calculations converge surprisingly slowly as the number of states included in the rotational band is increased, and that there are large variations in the intermediate un-converged calculations. We have found that, for symmetric-rotor nuclei with $K \neq 0$ that have ground state bands up to sufficiently large angular momenta, cal-

culation of the CN production cross sections requires at least the inclusion of states $I_{\max}$ up to $I \simeq I_{\mathrm{gs}} + 14$ in order to have converged results. This applies to both angle-integrated cross sections, and to elastic angular distributions, although only the former are discussed in this paper.

When the rotational excitation energies are small (the case of large moment of inertia, applicable to the actinide and rare-earth nuclei), we show that the converged CN production cross section is in fact very nearly independent of initial spin I, and independent of the band-head spin projection $K = I_{\mathrm{gs}}$ on the symmetry axis. This is also true for the total cross section and the sum of the elastic and all inelastic-channel cross sections. The 'very near' independence refers to deviations of less than 1%, and sometimes only 0.02%, that come from finite excitation energies.

In the adiabatic limit of *zero* excitation energies, we provide a rigorous proof that the angle-integrated cross sections discussed herein are *exactly* independent of both the initial spin I and band-head spin projection K. In the adiabatic limit, these quantities are simply the cross sections calculated for a fixed orientation of the deformed nucleus, averaged over all possible orientations. We conclude that rare-earth and actinide nuclei very nearly follow the adiabatic limit.

The independence of many important cross sections on K and I suggests that cross sections for $K > 0$ nuclei and/or cross sections for $I > I_{\mathrm{gs}}$ may be most simply and efficiently calculated by equivalent calculations with $I = K = 0$. This revisits the discussion of Lagrange *et al.* [2], where we conclude that the small difference they did find can be almost entirely attributed to insufficient convergence of their coupled-channels calculations.

We note several features that are relevant to applica-

*Electronic address: `dietrich2@llnl.gov`

tions of the present work. All of the coupled channels calculations carried out in this paper are for reactions on the ground and excited states of a single rotational band, assuming a rotational model and an optical potential that depends on incident neutron energy but not on the spectroscopic properties of the coupled states. The individual calculations directly apply to cases such as the ground *vs.* first-excited state of ^{239}Pu, since both states are members of the same $K = \frac{1}{2}$ band, but not to cases where the states belong to different bands (such as the ground and first-excited (76.5 eV) states of ^{235}U). The calculations certainly do not predict the cross sections for transitions between bands, since this requires excitation of the internal nuclear degrees of freedom rather than just the rotational excitations. However, the K-independence predicted by the adiabatic model and found to be a good approximation by the full calculations indicates that the absorption and total cross sections are very close even for states in different bands, as long as the optical potential is not dependent on the band properties. As discussed in Sec. V, there is very little experimental evidence for dependence on target spin in optical-model observables such as total cross sections and strength functions in low-energy neutron reactions. Some caution is necessary in making this assumption for estimating transmission coefficients for Hauser-Feshbach calculations of neutron-induced deexcitation of very high spin isomeric states, such as the 16^+ 2.45-MeV isomer in ^{178}Hf [3] or the 9^- isomer in ^{180}Ta near 77 keV [3, 4]. In such cases the optical potential, particularly its imaginary part, may be altered because of the reduced density of 2-particle 1-hole states that serve as doorways for the development of a compound system.

One situation in which the conclusions of this paper do not hold is the subbarrier absorption of charge particles. In this case excitation or deexcitation of the internal modes of the target by channel coupling can alter the effective height of the Coulomb barrier, which can significantly affect the absorption cross section. This effect has been explicitly studied for fusion from an excited state by Kimura and Takigawa [5], and has also been discussed in a general theory of heavy-ion fusion by Hussein [6].

This article is organized as follows: Sec. II shows results of the study we carried out of the convergence of the cross sections in actinide nuclei as a function of the number of coupled states. It also shows that when sufficient states are included in the calculation, the cross sections calculated with a target in its first-excited state are very close to those for the ground state. These results provide the motivation for a re-examination of the adiabatic approximation, which is described in Sec. III. Tests of the accuracy of the cross sections calculated in the adiabatic approximation and of its prediction that these cross sections are independent of the I and K quantum numbers are shown in Sec. IV for three regions of statically deformed nuclei: the actinides, deformed rare earths, and the s-d shell nuclei. The summary and conclusions are presented in Sec. V. Some details of the formalism used

in Sec. III and of the numerical calculations are shown in Appendix A, and the optical potential used in the rare-earth calculations is described in Appendix B.

II. CONVERGENCE OF COUPLED-CHANNEL CALCULATIONS

In the early days of the development of coupled channel calculations, computations of neutron scattering on deformed nuclei were carried out either in the adiabatic approximation or with only a few coupled levels (see, for example, Refs. [7, 8]). In fact, until the past decade, calculations on rare-earth and actinide nuclei carried out as input for Hauser-Feshbach calculations typically coupled only three states in a ground state band of an even-even nucleus, for which $K = 0$, and five states in odd-mass nuclei. In a more recent careful study of the convergence of such calculations, Sukhovitskii *et al.* [9] found that for scattering on ^{238}U, it was necessary to extend the coupling scheme to five levels in order to achieve a stable result (*i.e.* one in which adding additional levels yields negligible changes in important quantities such as the total and compound-nuclear formation cross sections σ_{cmpd}).

In the present work, in which a major goal is to establish the connection between the values of σ_{cmpd} for reactions with neutrons incident on the ground state of a nucleus and those for an excited-state target, we have found it necessary to revisit the question of convergence of the calculations as the number of coupled states N is increased. We find that coupling a sufficient number of states is crucial for getting an accurate result, and that for odd-mass nuclei in the actinide region as many as 14 states must be coupled.

In the calculations in this section we use the Flap 2.2 optical potential [10], which had been tuned to reproduce neutron total cross sections in the actinides with a minimal coupling scheme (3 levels for even-even targets). In view of our findings that a much larger coupling scheme is necessary to generate reliable cross sections on excited states, we intend to adjust this potential so that it is consistent with the extended coupling scheme.

A common set of deformation parameters was used for all of the actinide calculations in the present work. These parameters were adopted from the study of ^{238}U of Ref. [9] for $\beta_2 = 0.219$ and $\beta_4 = 0.053$; the small value of β_6 was ignored. These parameters were converted to deformation lengths δ_2 and δ_4 by multiplying them by the 7.8183 fm radius of the real central potential in Ref. [9], yielding $\delta_2 = 1.7122$ fm and $\delta_4 = 0.4144$ fm. For calculations on other actinides in the present work we scale the deformation lengths by $(A/238)^{1/3}$. These values of δ_2 and δ_4 were used to deform the real and imaginary central potentials; the spin-orbit potential was not deformed. We found that it was sufficient to expand the deformed optical potential up to a maximum Legendre-polynomial order of 6; the calculations in the actinide

and rare-earth regions were carried out with a maximum order of either 6 or 8. The calculations were carried out with the ECIS06 coupled-channel code [11], and checked with both the FRESCO code [12, 13] and the CoH$_3$ code [14].

Unless stated otherwise, the level schemes for the target states in the coupled-channels calculations were taken from their experimental values as reported in the ENSDF data base [3]. For all calculations, including those for reactions on excited states, the target states included in the calculation begin with the bandhead $I = K$ and include N levels that are consecutive in their spin I.

In this paper we are concerned only with angle-integrated cross sections. The compound formation cross section values σ_{cmpd} were obtained by subtracting the sum of the inelastic cross sections σ_{inel} from the reaction cross section σ_{reac}, where the latter is defined by the difference of the total and shape elastic cross sections, $\sigma_{tot} - \sigma_{elas}$.
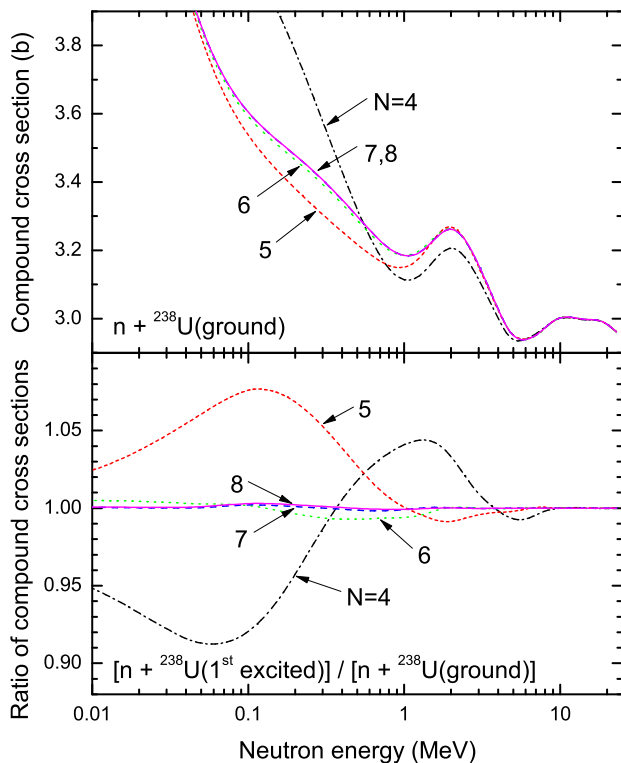

FIG. 1: Upper panel: dependence of compound formation cross sections for neutrons on ^{238}U on N, the number of coupled states. Lower panel: ratio of cross section for neutrons incident on the first excited state to that on the ground state. Note that the excited- to ground-state ratio is very close to unity when a sufficient number of levels is coupled.

The upper portion of Fig. 1 shows the convergence of the compound formation cross section σ_{cmpd} for neutrons on the $K = 0$ ^{238}U ground state as the number of coupled states N increases. The lower portion shows the corresponding ratios of the cross section for neutrons incident on the first-excited state to that on the ground

state. We see that for the chosen potential and deformation parameters at least 6 states must be coupled to yield stable results for σ_{cmpd} over the entire energy range. For the excited- to ground-state ratio, 7 to 8 states must be coupled, and the result is remarkably close to unity, with deviations of only a few tenths of a percent. In this as well as all other cases studied, the calculations for the various N converge at high energies, which is consistent with the known behavior of direct-interaction models for inelastic scattering (e.g. adiabatic and Born approximations).
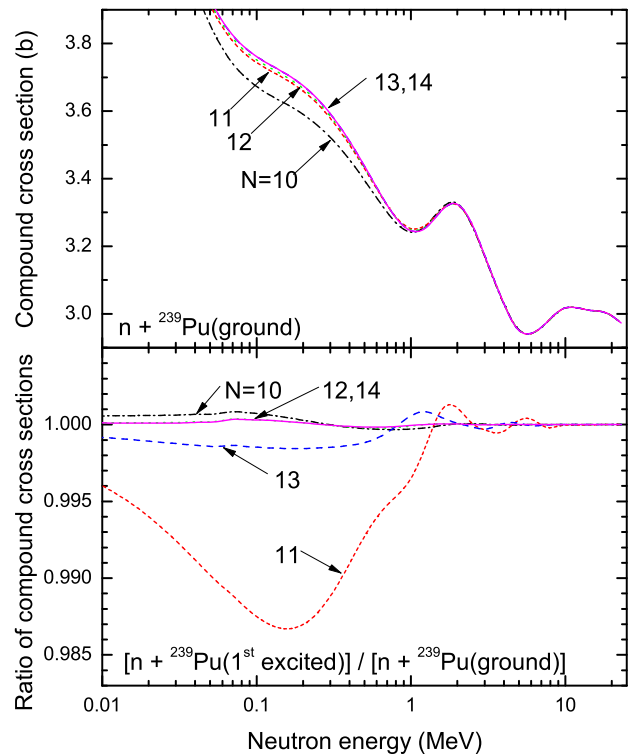

FIG. 2: Same as Fig. 1, but for ^{239}Pu. As for ^{238}U, the excited- to ground-state ratio is very close to unity when a sufficient number of levels is coupled.

Figure 2 shows the same information for ^{239}Pu, for which the ground state has $I = K = \frac{1}{2}$ and the 7.86-keV first-excited state has $I = \frac{3}{2}$. The results are similar to those for ^{238}U; however, for bands with $K \neq 0$, a much larger set of states is necessary. In the case of ^{239}Pu, 13 to 14 coupled states are required for the cross section on the ground state, and 14 for the excited- to ground-state ratio. Calculations with N=15 to 17 confirm that 14 states are sufficient. When fully converged, the excited to ground ratio is much closer to unity than for ^{238}U; note the greatly expanded vertical scale in the bottom part of the figure.

A curious feature of the approach to stability with increasing N, evident in the lower portion of Fig. 2, is the odd-even staggering of the ratios. That is, the calculations with even N are systematically closer to the converged value than those for the adjacent odd N. This is
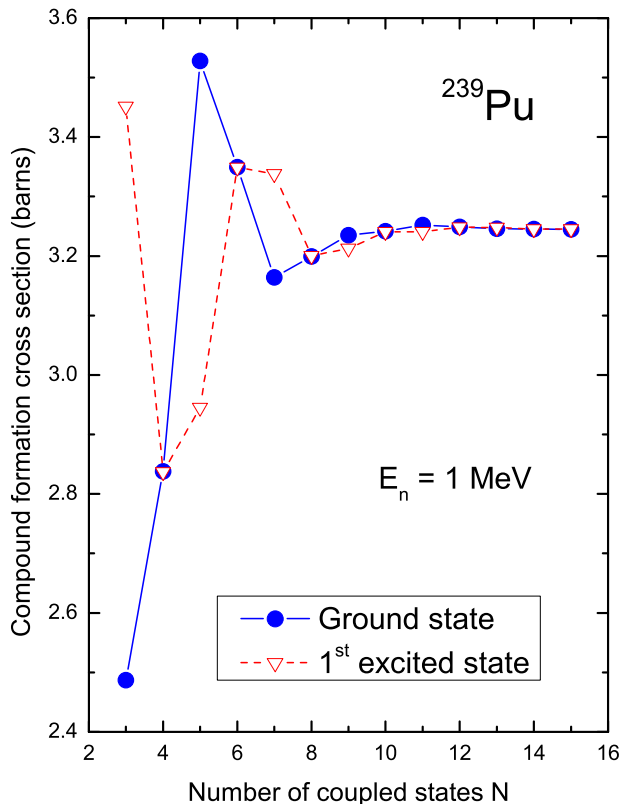
FIG. 3: Calculated compound formation cross sections at 1 MeV incident energy for neutron on the ground (filled circles) and first excited (open triangles) states of ^{239}Pu, as a function of the number of coupled states.
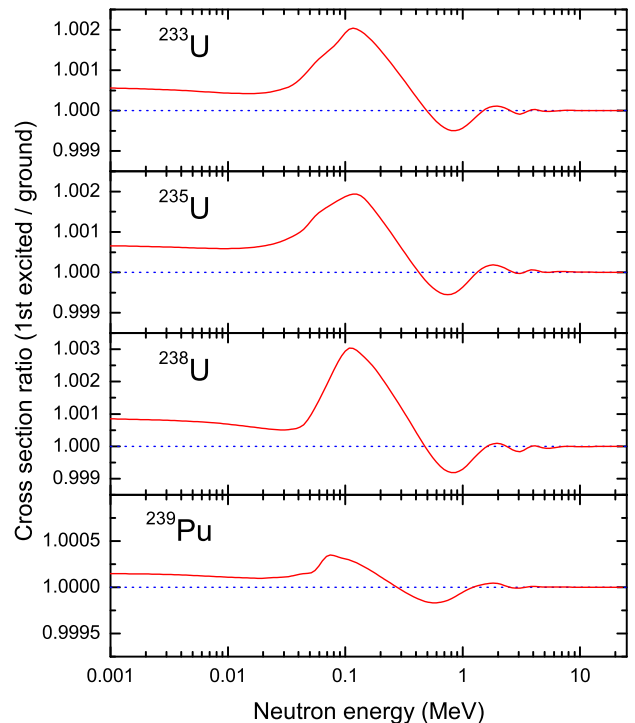

FIG. 4: Ratio of compound formation cross sections on the first-excited and ground states for four nuclei with different ground-state spins: ^{233}U ($\frac{5}{2}^+$), ^{235}U ($\frac{7}{2}^-$), ^{238}U (0^+), and ^{239}Pu ($\frac{1}{2}^+$). In these calculations sufficient levels are coupled to ensure the reliability of these ratios, which are very close to unity. Note in particular the highly expanded vertical scale for ^{239}Pu.

further illustrated in Fig. 3, which shows the values of σ_{cmpd} as a function of N separately for ground and first-excited targets, at a specific incident energy (1 MeV). For even N, the two calculations are in agreement, even when the common value is quite different from the fully converged result. On the other hand, the two values for odd N are significantly different, at least until convergence is reached at high N. This behavior appears consistent with the signature selection rule for quadrupole matrix elements within rotational bands (see Eqs. (4-68a),(4-71) in Ref. [15]), which favors $\Delta I = 2$. In the present case, we see that the number of strong upward coupling matrix elements is the same when N is even, but differs for odd values of N. The same pattern is seen for ^{169}Tm (see Sec. IV B), which also is a $K = \frac{1}{2}$ nucleus with a very low-lying $I = \frac{3}{2}$ first excited state. However, this simple odd-even effect was not found in any of the other cases studied.

Figure 4 shows the fully converged first-excited to ground-state ratios of σ_{cmpd} for four actinide nuclei covering a range of K values. The cases shown are ^{233}U ($\frac{5}{2}^+$), ^{235}U ($\frac{7}{2}^-$), ^{238}U (0^+), and ^{239}Pu ($\frac{1}{2}^+$). We find that $N = 14$ is sufficient to achieve convergence for the odd-mass nuclei (for which $K \neq 0$), and have used this value in the calculations shown in the figure. For ^{238}U we

have used $N = 8$. We see that all deviations of the ratio from unity are small, not exceeding 0.3%. The energy dependence of the deviation has a similar shape for all four cases, and the deviations damp out quickly above 1 MeV. There are no features of the energy dependence that are clearly correlated with the opening of specific inelastic channels in the various nuclei.

Most of the excited-state cross sections in the present work refer to the first excited state within a band. The very small deviations of this ratio from unity raise the question of whether the same result holds for targets in higher excited states. We show an example of the excited/ground ratio for neutrons incident on the second excited state of ^{238}U in Fig. 5, along with the corresponding result for the first excited state that was shown in Fig. 4. We chose $N = 10$ for these calculations to ensure convergence. We see that the deviations from unity of the second excited state calculation are larger than those for the first excited state by an amount very roughly consistent with the 10/3 ratio of excitation energies. The deviations from unity are still small, remaining below 1%.

The near equality of cross sections on the ground and excited states of a given nucleus that is uncovered when sufficient levels of a rotational band are coupled has its
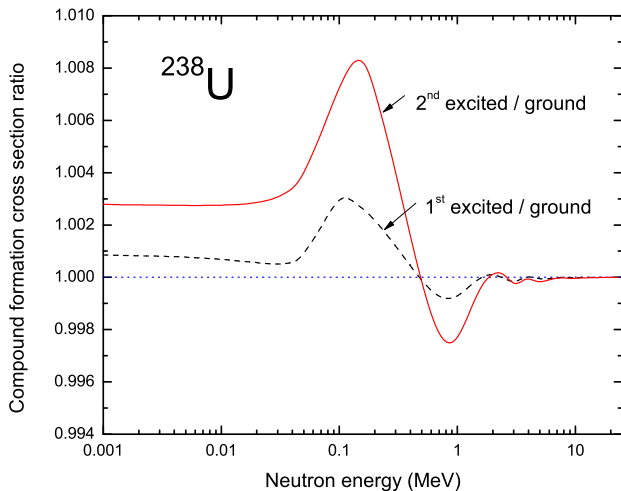
FIG. 5: Solid curve: ratio of compound cross sections on the second excited state of ^{238}U to that on the ground state. Dashed curve: same, for the first excited state. The deviation of the ratio from unity scales roughly as the excitation energy.

origin in the adiabatic approximation for scattering from deformed nuclei. This approximation is discussed in the next section.

III. ADIABATIC MODEL

A. General expressions for the cross sections

Before dealing with the adiabatic model and other approximations, it is useful to exhibit general expressions that relate the scattering wave functions and the coupled-channels scattering potential to the cross sections of interest in this paper. The total cross section may be written as the sum of two terms. One of these is the compound formation cross section, and the other is the sum of the scattering cross sections to all of the explicitly coupled channels, which we call the direct cross section:

$$\sigma_{tot} = \sigma_{cmpd} + \sigma^{dir}. \qquad (1)$$

The direct cross section may be further divided into the shape elastic cross section σ_{elas}^{dir} and the sum of cross sections to all of the remaining directly coupled states, σ_{inel}^{dir}:

$$\sigma^{dir} = \sigma_{elas}^{dir} + \sigma_{inel}^{dir}. \qquad (2)$$

We choose a linear-momentum representation in which the noninteracting states of a coupled-channels system are represented by $|\mathbf{k}a\rangle$, where $\hbar\mathbf{k}$ is the relative momentum of the projectile and target, and a represents all intrinsic quantum numbers of the projectile and target required to specify a given channel. We define a non-interacting Hamiltonian H_0, which includes the relative kinetic energy of the projectile and target, as well as the

sum of their masses in a particular channel a, including their internal excitation energies. The Schrödinger equation for the noninteracting pair in channel a is

$$(E - H_0)|\mathbf{k}a\rangle = 0. \qquad (3)$$

For the noninteracting solutions, we use plane waves normalized to unity in a large box of volume Ω with periodic boundary conditions, so that the noninteracting wave functions in the coordinate representation are

$$\langle \mathbf{r}a'|\mathbf{k}a\rangle = \Omega^{-1/2}\, e^{i\mathbf{k}\cdot\mathbf{r}}\, \delta_{a'a}. \qquad (4)$$

We may also choose to add a constant offset to H_0 so that the energy E corresponds to the relative projectile-target kinetic energy in a particular channel a of a coupled system.

To describe the full coupled-channels problem, we introduce an interaction $U = V + iW$, which is not Hermitian and can also couple channels distinguished by different values for the parameters a. The components V and W are separately Hermitian and are to be identified with the real and imaginary parts of a deformed optical potential. The Schrödinger equation for the fully interacting state that develops from an initial state $|\mathbf{k}a\rangle$ when the interaction U is turned on is

$$(E - H_0 - U)|\psi_{\mathbf{k}a}^{(+)}\rangle = 0. \qquad (5)$$

The $(+)$ superscript indicates the solution that contains a plane wave in the incident channel a, together with outgoing scattered waves in the incident channel as well as all other channels coupled to it via U. Because of the coupling represented by U, the state vector $|\psi_{\mathbf{k}a}^{(+)}\rangle$ contains components in all coupled channels, not just the incident channel; the subscript $\mathbf{k}a$ and superscript $(+)$ simply indicate the boundary conditions imposed on the solution of Eq. (5). This can be made explicit by writing the wave function in a coordinate representation,

$$\langle \mathbf{r}a'|\psi_{\mathbf{k}a}^{(+)}\rangle = \psi_{a';\mathbf{k}a}^{(+)}(\mathbf{r}), \qquad (6)$$

which can be viewed as a column vector with channel indices a'. Similarly, the interaction can be written (for a local potential) as

$$\langle \mathbf{r}a|U|\mathbf{r}'a'\rangle = U_{aa'}(\mathbf{r})\, \delta(\mathbf{r} - \mathbf{r}'), \qquad (7)$$

which is a matrix in the channel indices a, a'. The usual set of coupled differential equations is obtained by multiplying Eq. 5 on the left by $\langle \mathbf{r}a'|$, and inserting a complete set $1 = \sum_{a''}\int d\mathbf{r}''|\mathbf{r}''a''\rangle\langle\mathbf{r}''a''|$ to the right of U. In numerical calculations, a partial-wave expansion and a recoupling to states of total angular momentum and parity is normally made, but this is not necessary for our purposes.

We will make use of the Lippman-Schwinger equation, which is equivalent to the above Schrödinger equation with the specified boundary conditions. It relates the

fully interacting solution to the noninteracting solution as

$$|\psi_{\mathbf{k}a}^{(+)}\rangle = |\mathbf{k}a\rangle + G_0^{(+)}U|\psi_{\mathbf{k}a}^{(+)}\rangle, \qquad (8)$$

in which $G_0^{(+)}$, the outgoing-wave Green's function for the noninteracting system, is given by

$$G_0^{(+)} = (E - H_0 + i\epsilon)^{-1}, \qquad (9)$$

where ϵ is a positive infinitesimal quantity. Note that $G_0^{(+)}$ does not couple different channels.

Using the above definitions, we can write the needed expressions for σ_{cmpd} and σ^{dir}. These expressions are derived in Appendix A. The compound formation cross section is

$$\sigma_{cmpd} = -\frac{\Omega}{k}\frac{2\mu_a}{\hbar^2}\,\text{Im}\,\langle\psi_{\mathbf{k}a}^{(+)}|U|\psi_{\mathbf{k}a}^{(+)}\rangle \qquad (10)$$

$$= -\frac{\Omega}{k}\frac{2\mu_a}{\hbar^2}\,\langle\psi_{\mathbf{k}a}^{(+)}|W|\psi_{\mathbf{k}a}^{(+)}\rangle, \qquad (11)$$

and the direct cross section is

$$\sigma^{dir} = -\frac{\Omega}{k}\frac{2\mu_a}{\hbar^2}\,\text{Im}\,\langle\psi_{\mathbf{k}a}^{(+)}|U^\dagger G_0^{(+)}U|\psi_{\mathbf{k}a}^{(+)}\rangle \qquad (12)$$

$$= \frac{\pi\Omega}{k}\frac{2\mu_a}{\hbar^2}\,\langle\psi_{\mathbf{k}a}^{(+)}|U^\dagger\delta(E-H_0)U|\psi_{\mathbf{k}a}^{(+)}\rangle. \qquad (13)$$

Expressions similar to Eqs. (10) and (11) frequently occur in scattering problems involving complex potentials. Examples related to the present work include an early expression for the s-wave neutron strength function by Porter [16], which was further studied by Cugnon [17]. Schiff [18] obtained the same expression in a study of the optical theorem in the presence of a complex scattering potential. Further studies by Hussein and collaborators [6, 19, 20] have considered complex potentials and the effects of channel coupling on absorption. The derivation in Appendix A yields results close to those in [20], and our results are compared with that work in the Appendix. The expressions above for σ_{cmpd} are also correct for charged incident particles, but those for σ^{dir} are not, due to the Coulomb divergence in the elastic cross section.

B. The adiabatic approximation for rigid rotors

We treat the situation in which the projectile interacts with the target through an axially deformed, parity conserving complex interaction $U = V + iW$ that does not depend on the spin or other internal quantum numbers of the target. With this assumption, the only dependence on these quantum numbers appears in the symmetric-top rotational wave functions [15]

$$\langle\omega|IMK\rangle = \sqrt{\frac{2I+1}{8\pi^2}}\,(-1)^{K-M}\,\mathcal{D}_{MK}^I(\omega), \qquad (14)$$

where I is the spin of the target state, and M and K are its projections on the space-fixed z-axis and the body-fixed symmetry axis, respectively. We employ the definition of Edmonds [21] for the rotation matrices $\mathcal{D}_{MK}^I(\omega)$, where $\omega = (\alpha, \beta, \gamma)$ represents the set of Euler angles required to rotate the space-fixed axes of the deformed target into the body-fixed axes[1]. Eq. 14 also defines the coefficients of a transformation between an angular (ω) and angular-momentum (IMK) representation for states in the space of target orientations. For an ideal axially-symmetric rotor, the excitation energy of an excited state of spin I above the bandhead is

$$E_I - E_K = \frac{\hbar^2}{2\,\mathcal{J}}\left[I(I+1) - K(K+1)\right], \qquad (15)$$

where $\mathcal{J}$ is the moment of inertia about an axis perpendicular to the symmetry axis. For $K = \frac{1}{2}$, there is an additional term due to Coriolis coupling [15], which is also inversely proportional to $\mathcal{J}$.

For the present case we replace the asymptotic quantum numbers $\mathbf{k}a$ by $\mathbf{k}IMK$, where we explicitly show the spin quantum numbers of the target state, but suppress the projectile quantum numbers. In this paper we are interested in the case where the target is unpolarized, so we will calculate the compound cross section averaged over the target spin projections M:

$$\langle\sigma_{cmpd}\rangle_M = -\frac{\Omega}{k}\frac{2\mu_a}{\hbar^2}\frac{1}{2I+1}\sum_M\langle\psi_{\mathbf{k}IMK}^{(+)}|W|\psi_{\mathbf{k}IMK}^{(+)}\rangle. \qquad (16)$$

We do not impose restrictions on the polarization state of the projectile, and in principle appropriate averages should be taken over the substates of the projectile. However, the main conclusion that in the adiabatic approximation certain cross sections are independent of the I and K quantum numbers of the target is independent of the polarization of the projectile.

The adiabatic approximation was developed and applied early in the history of coupled-channel problems [7, 8, 23, 24], presumably because it is computationally economical compared to the exact solution. It appears to have fallen into disuse with the development of computers with sufficient memory and speed to carry out the full solutions easily. In reexamining the adiabatic approximation for the present work, we have found that it

---

[1] The angles (α, β, γ) are identical to (ϕ, θ, ψ) as defined in Ref. [22], p. 76. The present notation avoids possible confusion with the scattering angles of the projectile. The phase of the symmetric-top wave function of Eq. (14) is identical to that of [15], p. 6; the extra factor $(-1)^{K-M}$ appears because the Bohr-Mottelson and Edmonds definitions of the rotation matrices differ by this factor. We also define a volume element for the Euler angles by $d\omega \equiv d\alpha\,\sin\beta\,d\beta\,d\gamma$, and a delta function by $\delta(\omega - \omega') \equiv \delta(\alpha - \alpha')\,\delta(\cos\beta - \cos\beta')\,\delta(\gamma - \gamma')$. The Euler-angle eigenvectors $|\omega\rangle$ form a complete orthonormal set; that is, $\langle\omega|\omega'\rangle = \delta(\omega - \omega')$ and $\int d\omega\,|\omega\rangle\langle\omega| = 1$.

provides useful insights into the target-state dependence of the total, direct, and compound-formation cross sections. We have also found that it can be more accurate than conventional solutions, if too few levels are included in the full-scale calculations to guarantee convergence of the results.

In the adiabatic approximation it is assumed that the moment of inertia is so large that the nuclear rotational motion can be considered frozen during the scattering, and consequently all states within a band become degenerate (see Eq. (15)). Thus, for scattering of a projectile incident on a target in a particular state $|IMK\rangle$, we replace the Lippman-Schwinger equation for the exact solution,

$$|\psi^{(+)}_{\mathbf{k}IMK}\rangle = |\mathbf{k}IMK\rangle + G_0^{(+)}U|\psi^{(+)}_{\mathbf{k}IMK}\rangle, \qquad (17)$$

by its limit as $\mathfrak{I} \to \infty$,

$$|\phi^{(+)}_{\mathbf{k}IMK}\rangle = |\mathbf{k}IMK\rangle + G_{ad,0}^{(+)}U|\phi^{(+)}_{\mathbf{k}IMK}\rangle, \qquad (18)$$

where $|\phi^{(+)}_{\mathbf{k}IMK}\rangle$ is the adiabatic approximation to the scattering state. The difference between $G_0^{(+)}$ and $G_{ad,0}^{(+)}$ is that in the latter the kinetic energy terms in the Hamiltonian corresponding to the target motion are absent, since they are proportional to $1/\mathfrak{I}$. We can also construct solutions for scattering from a target at fixed orientation ω in the adiabatic limit,

$$|\phi^{(+)}_{\mathbf{k}\omega}\rangle = |\mathbf{k}\omega\rangle + G_{ad,0}^{(+)}U|\phi^{(+)}_{\mathbf{k}\omega}\rangle. \qquad (19)$$

The desired solution, given by Eq. (18), can be expressed as a linear combination of the solutions to Eq. (19). To see this, we multiply Eq. (19) by the transformation coefficients $\langle\omega|IMK\rangle$ relating the angle and angular-momentum representations, and integrate over all values of ω,

$$\int d\omega\,|\phi^{(+)}_{\mathbf{k}\omega}\rangle\langle\omega|IMK\rangle = \int d\omega\,|\mathbf{k}\omega\rangle\langle\omega|IMK\rangle$$
$$+ \int d\omega\,G_{ad,0}^{(+)}U|\phi^{(+)}_{\mathbf{k}\omega}\rangle\langle\omega|IMK\rangle. \qquad (20)$$

By using the completeness relation for the Euler-angle eigenstates $|\omega\rangle$ in the first term on the right side of this equation, and noting that in the second term the operator $G_{ad,0}^{(+)}U$ may be taken outside the integral because it is independent of ω, we obtain

$$\int d\omega\,|\phi^{(+)}_{\mathbf{k}\omega}\rangle\langle\omega|IMK\rangle = |\mathbf{k}IMK\rangle$$
$$+ G_{ad,0}^{(+)}U\int d\omega\,|\phi^{(+)}_{\mathbf{k}\omega}\rangle\langle\omega|IMK\rangle. \qquad (21)$$

We compare this with Eq. (18) to find the key result

$$|\phi^{(+)}_{\mathbf{k}IMK}\rangle = \int d\omega\,|\phi^{(+)}_{\mathbf{k}\omega}\rangle\langle\omega|IMK\rangle \qquad (22)$$

$$= \int d\omega\,\sqrt{\frac{2I+1}{8\pi^2}}\,(-1)^{K-M}\,\mathcal{D}^I_{MK}(\omega)|\phi^{(+)}_{\mathbf{k}\omega}\rangle. \qquad (23)$$

We use this result to evaluate the compound formation cross section of Eq. (16) in the adiabatic approximation. Substituting Eq. (22) into the matrix element in Eq. (16) yields

$$\langle\phi^{(+)}_{\mathbf{k}IMK}|W|\phi^{(+)}_{\mathbf{k}IMK}\rangle = \int d\omega'\int d\omega \qquad (24)$$
$$\times\langle IMK|\omega'\rangle\langle\omega|IMK\rangle\langle\phi^{(+)}_{\mathbf{k}\omega'}|W|\phi^{(+)}_{\mathbf{k}\omega}\rangle.$$

Since the target orientation is fixed in $|\phi^{(+)}_{\mathbf{k}\omega}\rangle$, the operator W cannot change it; consequently W is local in ω. Moreover, the state vectors on either side of the matrix element are orthogonal unless $\omega' = \omega$. Thus the matrix element simplifies to[2]

$$\langle\phi^{(+)}_{\mathbf{k}IMK}|W|\phi^{(+)}_{\mathbf{k}IMK}\rangle = \qquad (25)$$
$$\int d\omega\langle IMK|\omega\rangle\langle\omega|IMK\rangle\langle\phi^{(+)}_{\mathbf{k}\omega}|W|\phi^{(+)}_{\mathbf{k}\omega}\rangle.$$

The sum over the target spin projections M is easily carried out using the properties of the rotation matrices [21],

$$\sum_M\langle IMK|\omega\rangle\langle\omega|IMK\rangle = \qquad (26)$$
$$\frac{2I+1}{8\pi^2}\sum_M\mathcal{D}^{I*}_{MK}(\omega)\mathcal{D}^I_{MK}(\omega) = \frac{2I+1}{8\pi^2}.$$

Combining Eqs. (16), (25), and (26), the final result is

$$\langle\sigma_{cmpd}\rangle_M = -\frac{\Omega}{k}\frac{2\mu_a}{\hbar^2}\frac{1}{8\pi^2}\int d\omega\,\langle\phi^{(+)}_{\mathbf{k}\omega}|W|\phi^{(+)}_{\mathbf{k}\omega}\rangle. \qquad (27)$$

This result for the M-averaged compound cross section in the adiabatic limit is simply the compound-formation cross section for scattering from a target at fixed orientation, averaged over all possible values of the Euler angles ω. There is no dependence on either the target spin I or the K-value of the band. This feature follows from the assumed independence of the optical potential U to these quantities, and of the averaging over the magnetic substates M of the target.

The preceding derivation does not depend on specific properties of W, and can be carried out for any valid operator in the adiabatic approximation (*i.e.* any operator that does not change the target orientation). Thus we obtain the direct cross section σ^{dir} by the substitution (compare Eqs. (11) and (13))

$$W \longrightarrow -\pi\,U^\dagger\,\delta(E-H_{ad,0})\,U, \qquad (28)$$

---

[2] Formally, we can represent W as $|\omega\rangle W(\omega)\langle\omega|$ in the target subspace, and we note that the state vector $|\phi^{(+)}_{\mathbf{k}\omega}\rangle$ can be represented as a product $|\chi^{(+)}_{\mathbf{k}\omega}\rangle|\omega\rangle$ of a scattering state in the projectile subspace and a state at fixed orientation ω in the target subspace. These observations, together with the orthogonality relation $\langle\omega'|\omega\rangle = \delta(\omega'-\omega)$, yield the stated result.

where the target rotational kinetic energy terms are absent in $H_{ad,0}$, the free Hamiltonian in the adiabatic limit. As in the derivation for σ_{cmpd}, we use the adiabatic-model condition that the above operator is diagonal in ω. Also as before, the adiabatic result for the M-averaged direct cross section is the average over all orientations of the cross section calculated for fixed ω, and is independent of I and K.

Since the total cross section σ_{tot} is the sum of σ_{cmpd} and σ^{dir}, its M-averaged value in the adiabatic limit will share their properties. Specifically, all three cross sections are independent of I and K of the target state. We note that this result does not require a partial wave expansion of the coupled-channels problem, or a specification of the polarization state of the projectile. It requires only an average over the magnetic substates of the target, which is assumed to be unpolarized.

In Ref. [2], an approximation was investigated in which the angular distributions for elastic and inelastic scattering to states of the same band in an odd-mass nucleus were expressed as linear combinations of the angular distributions for scattering on an even-even ($K = 0$) nucleus. Although not stated in [2], this relation also has its origin in the adiabatic approximation, and can be derived from the adiabatic-approximation scattering amplitude in [7]. The accuracy of this result should be studied further using adequately converged coupled-channels calculations, but this topic is beyond the scope of the present article, which is concerned with angle-integrated cross sections.

There are two approaches to implementing the adiabatic approximation. In one of these, the coupled equations are solved in the body-fixed frame. This method is significantly more efficient than the full (nonadiabatic) technique, which is why it was implemented early in the development of coupled channels calculations (e.g. Refs. [7, 8]). Alternatively, a full coupled-channels calculations can be made with all excitation energies set to the same value, and with a sufficient number of levels coupled to ensure convergence. This second approach was employed in the adiabatic calculations shown in this paper.

In the following section we will test the accuracy of the adiabatic-approximation prediction that the cross sections σ_{tot}, σ_{cmpd}, and σ^{dir} are independent I and K when applied to calculations using the full (nonadiabatic) coupled-channels technique.

IV. CROSS-SECTION DEPENDENCE ON I AND K

In this section we further investigate the validity of the adiabatic-approximation predictions in the actinide region. We also show results for deformed rare-earth nuclei, which should be expected to be similar to those in the actinides, but for smaller values of the moment of inertia. We also show calculations for a statically deformed

nucleus in the s-d shell region, ^{20}Ne.

A. Actinide nuclei

To study the validity of the independence of certain cross sections to the I and K quantum numbers, it is convenient to carry out calculations on a fictitious system we refer to as "^{238}U" that has level energies and quantum numbers chosen to illustrate specific points, but otherwise employs the optical potential and deformations for the actual ^{238}U described in Section II. We choose the excitation energy spectrum for a band of given K to be that of the ideal rotor of Eq. (15). It is well known that the moments of inertia are band-dependent, and that the $K = 0$ ground state bands of even-even nuclei have moments of inertia that are significantly smaller than those for bands with $K \neq 0$. We choose the value of the inertial parameter $\hbar^2/2\mathfrak{I}$ to be 0.006 MeV, which is between the physical values 0.0074 MeV for ^{238}U ($K = 0$), and 0.0052 MeV for ^{235}U ($K = \frac{7}{2}$). Unless otherwise indicated, this intermediate value of $\hbar^2/2\mathfrak{I}$ is applied for all K-values assumed for the fictitious "^{238}U". Using this common value of the inertial parameter allows us to study the K-dependence of the adiabatic-approximation predictions without the additional complication introduced by the actual band dependence of the moment of inertia.

Figure 6 shows the ratio of full coupled-channels (i.e. nonadiabatic) calculations to adiabatic calculations for σ_{cmpd}, σ^{dir}, and σ_{tot} on the bandheads of assumed $K = 0$ and $K = \frac{7}{2}$ bands in "^{238}U". These are the three cross sections that are independent of I and K in the adiabatic limit. The curves are for $K = 0$, and the points are for $K = \frac{7}{2}$. The adiabatic approximation is rather good for all three cross sections, since in all cases it is within approximately 2% of the true (nonadiabatic) result. The near equality of the results for $K = 0$ and $K = \frac{7}{2}$ shows that the K-independence prediction of the adiabatic approximation is well reflected in the nonadiabatic calculations.

The accuracy of the K-independence prediction is exhibited in more detail in Fig. 7, which shows the ratio of the compound cross sections for various K values (up to $K = 6$) to that for $K = 0$. The deviations from unity increase uniformly with increasing K, but do not exceed 0.2%. Calculations carried out for half-integral K fit smoothly between those for integral K, but for clarity are not shown.

Finally, in Fig. 8 we show the dependence on the inertial parameter $\hbar^2/2\mathfrak{I}$ (labeled c in the figure) of the nonadiabatic/adiabatic ratio for calculations on a $K = 0$ bandhead. The deviations from unity are roughly linear, at least up to the value 0.006 MeV we have adopted as a realistic average value of the inertial parameter.
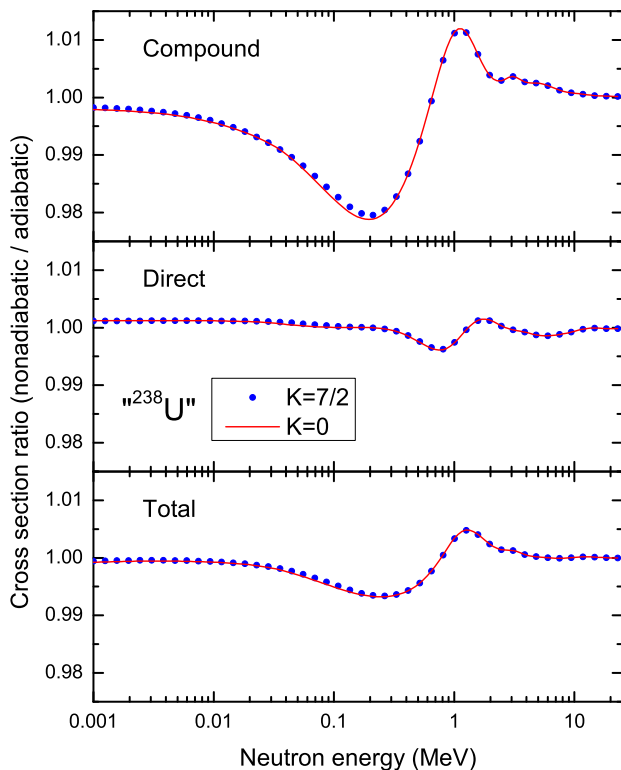
FIG. 6: Ratio of nonadiabatic to adiabatic calculations for σ_{cmpd}, σ^{dir}, and σ_{tot} on a pseudo-nucleus resembling ^{238}U except for the level structure (see text). The calculations assume neutrons incident on a $K = 0$ bandhead (solid curves) and a $K = \frac{7}{2}$ bandhead (points). The moment of inertia is the same for both cases, and in consequence the cross sections are nearly independent of K.

B.   Rare-earth nuclei

Like the actinides, the heavy rare-earth nuclei are understood to be rigidly deformed rotors, and thus it should be expected that many of the results we have found for the actinides should apply also to the deformed rare earth nuclei. The principal difference is that the moment of inertia is significantly smaller in the rare earths, as indicated by the level spacings in the ground-state band of even-even nuclei, which are roughly twice those in the actinides. We should therefore expect that the deviations from the adiabatic model should be somewhat larger in the rare earths than in the actinides, but should follow the same patterns. We show a small sample of results for calculations on three nuclei spanning the same range of K as for the actinide nuclei, ^{165}Ho $(\frac{7}{2}^-)$, ^{169}Tm $(\frac{1}{2}^+)$, and ^{170}Yb (0^+).

The optical potential used in these calculations is a regional potential developed for data evaluations in the rare earth region [25]. The parameterization of this potential is described in Appendix B. As for the potential used in the actinides, this potential was used in calculations with $N{=}3$ for even-even nuclei and $N{=}5$ otherwise;
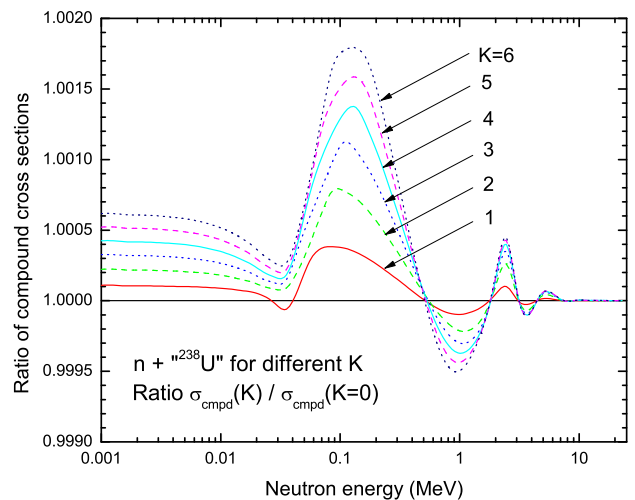

FIG. 7: Nonadiabatic calculations for the pseudo-nucleus "^{238}U", showing the ratio of compound cross sections on the bandhead for a given K value to that for $K = 0$. These results show that the deviation from the adiabatic model prediction of K-independence is very small; note the highly expanded vertical scale. Calculations with half-integral K fit smoothly between the values shown for integral K.
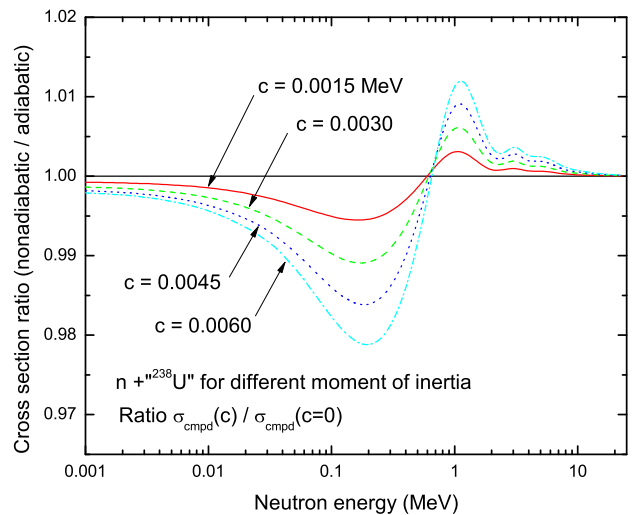

FIG. 8: Nonadiabatic/adiabatic ratio of the compound formation cross section for reactions on a $K = 0$ bandhead, for several values of the inertial parameter $c \equiv \hbar^2/2\mathcal{I}$. The values of c extend from 0, which is the adiabatic limit, up to 0.006, which represents a rough average of physical values for actinide nuclei. Note that these ratios are approximately linear in c, which determines the excitation energy scale.

this potential should therefore also be readjusted for calculations with an extended level scheme.

The deformation lengths were taken from the deformations measured for ^{166}Er by alpha scattering in Ref. [26]. This experiment, which studied a number of deformed rare earth nuclei, showed that the hexadecupole deformations in the region of interest to be very small, and

consequently we set δ_4 to zero. The quadrupole deformation lengths we adopt are given by $\delta_2 = 1.8202(A/166)^{1/3}$ fm, which incorporates a scaling as $A^{1/3}$, as was done in the actinide calculations.

The calculations in the rare earth region were carried out with experimentally-determined level schemes, taken from ENSDF [3]. Since the ENSDF compilation contains only 12 levels for the ^{169}Tm ground-state band and we wish to carry out calculations with up to 14 coupled levels, we have added two levels by extrapolation of the known levels; these levels are at excitation energies 2.038 MeV $(25/2)^+$ and 2.163 MeV $(27/2)^+$.

Using the above parameters, the calculations were carried out exactly as for those in the actinides using the ECIS06 code, expanding the potential to Legendre-polynomial order 8. We do not show details of the convergence as a function of the number of coupled states N, but the results are similar to those in the actinides. As before, we find that $N = 8$ for $K = 0$ bands and $N = 14$ for $K \neq 0$ is sufficient to ensure convergence of the excited- to ground-state ratios. Also, the pronounced variations in the excited to ground state ratio for even *vs.* odd N observed for ^{239}Pu and shown in Fig. 3 were repeated for ^{169}Tm.
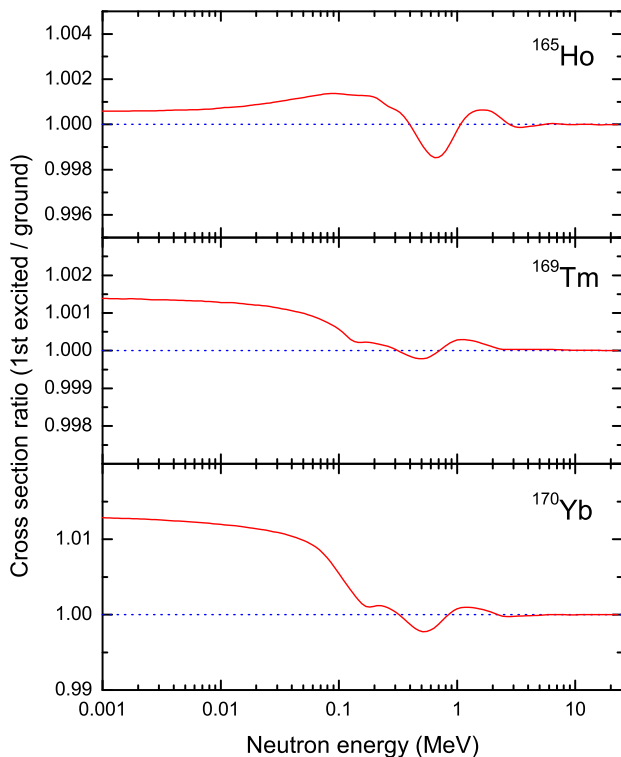

FIG. 9: Ratio of compound formation cross sections on the first excited state to those on the ground state for three deformed rare-earth nuclei, ^{165}Ho $(\frac{7}{2}^-)$, ^{169}Tm $(\frac{1}{2}^+)$, and ^{170}Yb (0^+).

The results for the compound formation cross sections are shown in Fig. 9 for the first-excited to ground state ratios, and Fig. 10 for the ratio of nonadiabatic to adia-
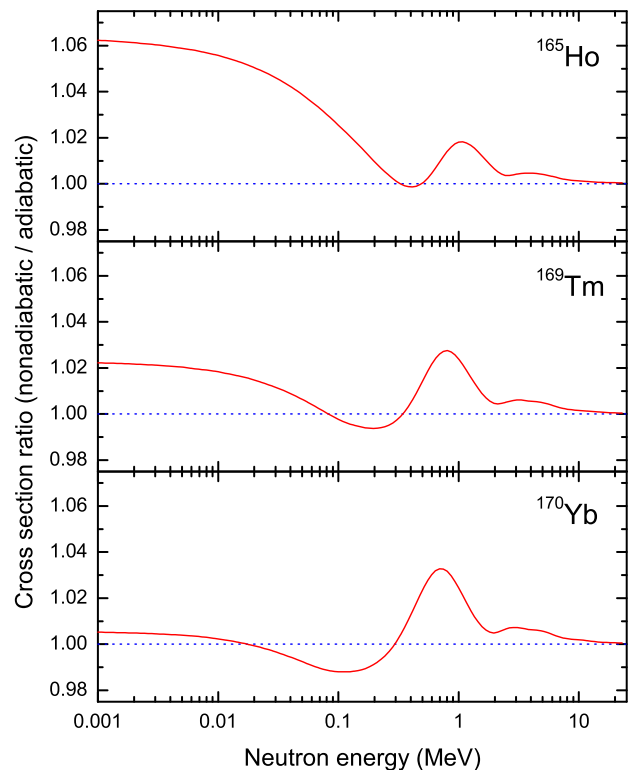

FIG. 10: Same as for Fig. 9, but for the ratio of nonadiabatic to adiabatic calculations for neutrons incident on the ground state of each target.

batic calculations on the bandheads.

As seen in Fig. 9, the deviations of the excited- to ground-state ratios from the adiabatic limit are small, but not as small as for the actinides. The deviation is of the order of 1% at low energies for ^{170}Yb, but for the other two nuclei the deviations are significantly smaller (approximately 0.1% or less). These results indicate that the compound formation cross sections shown in Fig. 3 of [1] for the ground and first excited states should be closer together in a fully converged calculation. The values for the nonadiabatic to adiabatic ratios of Fig. 10 show deviations of a few percent from the adiabatic limit, as in the actinides. However, we note that this deviation is as large as 6% for ^{165}Ho at low energies.

C. *s-d* shell nuclei

A more severe test of the adiabatic approximation should be provided by the deformed light nuclei in the *s-d* shell, such as ^{20}Ne. This isotope has a 2^+ state at 1.63 MeV, defining a good rotational band at least to the 8^+ state at 15.8 MeV. These energies indicate a much smaller moment of inertia than the actinide and rare-earth nuclei discussed above, and so we might expect much larger deviations of the non-adiabatic calculations compared with the results in the adiabatic limit. For our calculations,

the neutron-^{20}Ne optical potential used was the global potential of Koning and Delaroche [27], in conjunction with the deformation parameters of Ref. [28]. The potential was evaluated at 5 MeV and used at all energies up to 50 MeV with nonrelativistic kinematics; this treatment should be sufficient to exhibit the state dependence of the cross sections, but is not intended as a realistic calculation of their absolute values.

Figure 11 shows first the results for coupled-channels up to the 8^+ state, where curves show the ratio of cross sections for the first excited state to those for the ground state. We see that the compound nucleus cross sections agree within 3%, and the direct reaction totals agree to better than 1%. Convergence is in fact obtained once the 6^+ state is included, but the final ratios are still surprisingly close to unity. Fig. 11 directly compares the non-adiabatic and adiabatic cross sections for the ground state. As expected, the ratio of these is further from unity than for the heavier nuclei, but still within 4% at almost all the incident energies.
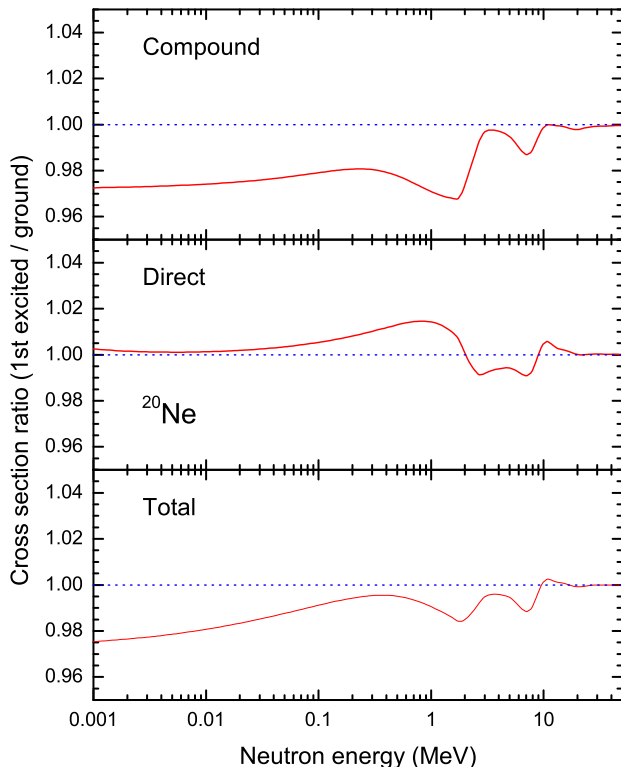

FIG. 11: Ratio of the cross sections σ_{cmpd}, σ^{dir}, and σ_{tot} on the first excited state to those on the ground state for the deformed s-d shell nucleus ^{20}Ne.

V. DISCUSSION AND CONCLUSIONS

Using standard coupled-channels calculations, we have investigated the behavior of the total, compound formation, and direct (elastic plus summed inelastic) cross
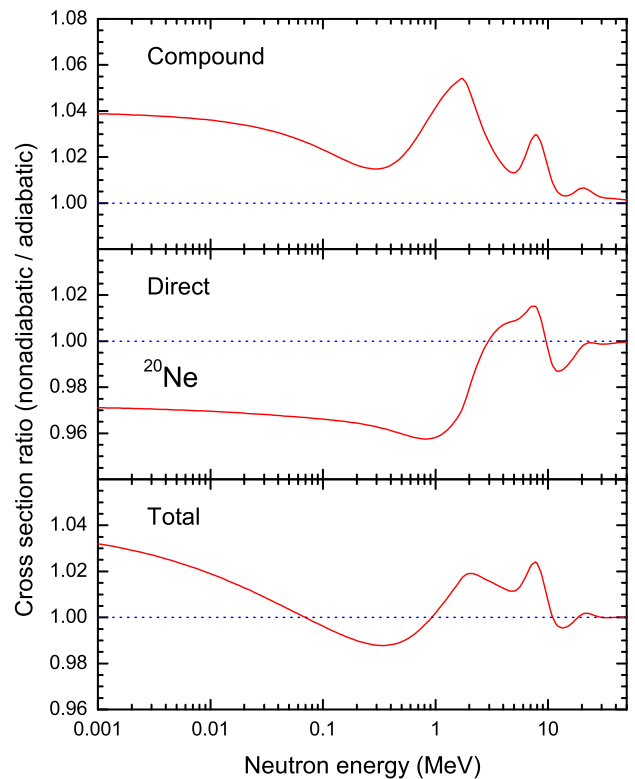

FIG. 12: Same as for Fig. 11, but for the ratio of nonadiabatic to adiabatic calculations on a ground-state target for each of the cross sections.

sections for neutrons incident on the ground and first-excited states of statically deformed nuclei in the actinides, the rare-earth region, and s-d shell nuclei. In all of these regions, the ratio of excited- to ground-state cross sections is very close to unity. The deviations from unity extend from about 2% in the s-d shell example (^{20}Ne) to less than 0.1% is the heaviest nuclei. It was essential to include sufficient levels in the coupled-channels calculations to achieve stable results; in the actinides and rare earths, we require 8 levels for $K = 0$ bands and 14 for $K \neq 0$.

Our results are consistent with those of Sukhovitskii et al. [9], who studied the convergence of neutron cross sections on ^{238}U as the number of coupled target states was increased, and found that if too few states were included significant errors could be incurred in important cross sections, such as the compound formation cross section (see Fig. 10 of Ref. [9]). In particular, the common practice of calculating neutron cross sections with 3 coupled levels in $K = 0$ bands was shown to be inadequate. The present work shows that one can also obtain poor results in bands with $K \neq 0$ when only 5 levels are coupled, which has also been common practice. Optical potentials whose parameters were determined with a restricted set of coupled states, including those used in the actinide and rare-earth calculations here, will need to be readjusted when an adequately large set of states is incorporated.

The nearly equal cross sections for ground and excited-state targets has led us to reexamine the adiabatic approximation for scattering on deformed nuclei. We have shown that in this model the total, compound, and direct cross sections are independent of the spin of the target state, I, as well as of the K-value of the band of which it is a member. We have tested the accuracy of the adiabatic approximation by comparing it with full coupled-channels calculations, and find that in all cases it is within a few percent of the exact results. In many cases this is comparable to or better than the accuracy of experiments. In the actinides and rare earths, the excited/ground ratio is in significantly better agreement with the adiabatic approximation than the ground-state cross sections.

Our conclusion that the adiabatic approximation is rather accurate provides a connection between cross-section calculations in the spherical and deformed regions of the isotopic table. In both cases the optical potentials normally employed are independent of the target spin. This implies the assumption that the projectile interacts with the nuclear density as a whole, and is essentially independent of the specific structural properties of the valence particle (or particles) that account for the spin (or K for deformed systems). In a spherical calculation one assumes the target spin is zero. However, in coupled-channels calculations for deformed nuclei it is necessary to include the K-value of the target band explicitly in the wave function, even though it is not included in the potential. In the adiabatic approximation the cross sections of interest in this paper are independent of K; this provides the connection between the spherical and deformed systems. This picture is supported by experimental evidence from neutron total cross section measurements. For nuclei usually treated as spherical, such measurements show little evidence for dependence on the spin of the target; see, for instance, the extensive measurements from LANSCE/WNR [29, 30]. The same is true for measurements in the actinides [31]. In both cases, the total cross sections for odd-mass nuclei are close (*i.e.* within experimental uncertainties) to those for neighboring even-even nuclei. Thus the target spin appears to act as an inert spectator in both spherical and deformed cases, and this is confirmed in the adiabatic approximation.

A frequently stated condition for the validity of the adiabatic approximation is that the projectile energy be large compared to the excitation energy of the most important target excitations. Clearly this requirement is too stringent, since, as is evident in the present work, the adiabatic approximation gives good results even down to the lowest energies where the condition is certainly not satisfied. A qualitative argument for the validity of the approximation at low energies is that most of the interaction of the projectile with the target, and in particular the coupling to other target states, takes place after the projectile has been sufficiently accelerated by the attractive nuclear potential for the approximation to be appropri-ate. A quantitative implementation of this idea has been suggested by Bohr and Mottelson (Ref. [15], Sec. 5A-2), in which an adiabatic treatment for the wave function is carried out inside the nucleus and matched at the nuclear boundary to wave functions in the external region which are treated nonadiabatically (*i.e.* with physical values for the target excitations). This approach has been used for estimating *s*-wave strength functions in deformed nuclei [32].

We conclude with some comments on the implications of the present work for practical calculations. The findings in this paper apply to the transmission coefficients used in Hauser-Feshbach calculations, since they are essentially a decomposition of σ_{cmpd} into components with fixed total angular momentum and parity. The same conclusions regarding approximate independence of σ_{cmpd} to I and K apply. We do not advocate using adiabatic calculations routinely, as long as the full coupled-channels calculations are carried out with a sufficient number of states. However, calculations on states with $K \neq 0$ can be time consuming, and the present work suggests that the cross sections and transmission coefficients can be calculated (at least in the deformed actinide and rare-earth nuclei) with a fictitious even-even (*i.e.* $K = 0$) model for the target, in which the moment of inertia is chosen the same as for the actual target. This is the approximation that was studied by Lagrange *et al.* [2]. While in some cases that work showed significant differences between the actual calculations and the fictitious even-even model at low energies ($\approx$1 MeV), it appears that coupling sufficient levels removes these discrepancies.

Appendix A: Calculation of compound and direct cross sections

In this appendix we derive the expressions for the compound-nuclear formation and direct cross sections, Eqs. (10)-(13) of Section III, using the definitions introduced in that section.

We begin by noting the relation between the total cross section in the incident state $\mathbf{k}a$ and the forward scattering amplitude given by the optical theorem,

$$\sigma_{tot} = \frac{4\pi}{k} \operatorname{Im} f_{\mathbf{k}a,\mathbf{k}a}. \tag{A1}$$

This is a very general result that applies to any wave

scattering problem whose amplitude at sufficiently large distances from the scatterer (apart from an overall normalization) can be written as

$$A(\mathbf{r}) = e^{i\mathbf{k}\cdot\mathbf{r}} + \frac{e^{ikr}}{r} f_{\mathbf{k}',\mathbf{k}}, \qquad (A2)$$

where $|\mathbf{k}'| = |\mathbf{k}| = k$. Ref. [33] summarizes a remarkably simple argument of van de Hulst [34] that derives the optical theorem from Eq. (A2) by considering the depletion of the intensity $|A(\mathbf{r})|^2$ at forward angles due to interference between the the incident and scattered waves. The essential features of a specific problem are contained in the calculation of the scattering amplitude. In the present case these features are the complex interaction U and the presence of multiple channels coupled by this interaction[3].

The T-matrix for scattering from the state $\mathbf{k}a$ to the state $\mathbf{k}'a'$ is

$$T_{\mathbf{k}'a',\mathbf{k}a} = \langle \mathbf{k}'a'|U|\psi_{\mathbf{k}a}^{(+)}\rangle, \qquad (A3)$$

which is related to the scattering amplitude $f_{\mathbf{k}'a',\mathbf{k}a}$ by

$$f_{\mathbf{k}'a',\mathbf{k}a} = -\frac{\Omega}{4\pi}\frac{2\mu_{a'}}{\hbar^2} T_{\mathbf{k}'a',\mathbf{k}a}, \qquad (A4)$$

where $\mu_{a'}$ is the reduced mass in channel a'. The scattering amplitude has been defined so that the differential cross section is

$$d\sigma_{\mathbf{k}'a',\mathbf{k}a}/d\hat{\mathbf{k}}' = (v'/v)\,|f_{\mathbf{k}'a',\mathbf{k}a}|^2, \qquad (A5)$$

where we denote the element of solid angle in the direction of $\mathbf{k}'$ by $d\hat{\mathbf{k}}'$. The relative velocities of the interacting particles in the initial and final states are denoted by v and v', respectively. Using the optical theorem, the total cross section for incident channel $\mathbf{k}a$ can be related to the T-matrix element by

$$\sigma_{tot} = \frac{4\pi}{k}\operatorname{Im} f_{\mathbf{k}a,\mathbf{k}a} = -\frac{\Omega}{k}\frac{2\mu_a}{\hbar^2}\operatorname{Im}\langle \mathbf{k}a|U|\psi_{\mathbf{k}a}^{(+)}\rangle. \quad (A6)$$

The T-matrix element in the last equation can be recast by eliminating $|\mathbf{k}a\rangle$ in favor of $|\psi_{\mathbf{k}a}^{(+)}\rangle$ with the help of the Lippman-Schwinger equation (Eq. (8)):

$$\langle \mathbf{k}a|U|\psi_{\mathbf{k}a}^{(+)}\rangle = \qquad (A7)$$
$$\langle \psi_{\mathbf{k}a}^{(+)}|U|\psi_{\mathbf{k}a}^{(+)}\rangle - \langle \psi_{\mathbf{k}a}^{(+)}|U^{\dagger}G_0^{(+)}U|\psi_{\mathbf{k}a}^{(+)}\rangle^*.$$

We take the imaginary part of this equation and insert it in Eq. (A6), which yields the result

$$\sigma_{tot} = -\frac{\Omega}{k}\frac{2\mu_a}{\hbar^2}\operatorname{Im}\langle \psi_{\mathbf{k}a}^{(+)}|U|\psi_{\mathbf{k}a}^{(+)}\rangle \qquad (A8)$$
$$-\frac{\Omega}{k}\frac{2\mu_a}{\hbar^2}\operatorname{Im}\langle \psi_{\mathbf{k}a}^{(+)}|U^{\dagger}G_0^{(+)}U|\psi_{\mathbf{k}a}^{(+)}\rangle.$$

---

[3] Note that since any open coupled channels are distinguishable from the elastic channel, they will not contribute to the interference between incident and scattered waves that leads to the optical theorem. Thus Eq. (A1) is valid even in the presence of channel coupling.

We will now show that the first term in this expression is the compound-nuclear formation cross section, σ_{cmpd}, and the second is the direct interaction cross section, σ^{dir}.

We begin this demonstration by making an explicit calculation of the direct cross section as the sum over all final states coupled by the interaction U, including both elastic and inelastic scattering. We use the Fermi golden rule for the transition probability per unit time to a given final state,

$$w_{\mathbf{k}'a',\mathbf{k}a} = \frac{2\pi}{\hbar}|T_{\mathbf{k}'a',\mathbf{k}a}|^2\delta(E_{\mathbf{k}a} - E_{\mathbf{k}'a'}). \qquad (A9)$$

The energies of the initial and final states are $E_{\mathbf{k}a}$ and $E_{\mathbf{k}'a'}$; the delta function constrains these to a common value, which we refer to below as E. We divide the transition probability by the nonrelativistic incident flux, $(1/\Omega)(\hbar k/\mu_a)$, to yield the cross section to get from state $\mathbf{k}a$ to $\mathbf{k}'a'$,

$$\sigma_{\mathbf{k}'a',\mathbf{k}a} = \pi\frac{\Omega}{k}\frac{2\mu_a}{\hbar^2} \qquad (A10)$$
$$\times\ \langle \psi_{\mathbf{k}a}^{(+)}|U^{\dagger}|\mathbf{k}'a'\rangle\,\delta(E_{\mathbf{k}a} - E_{\mathbf{k}'a'})\,\langle \mathbf{k}'a'|U|\psi_{\mathbf{k}a}^{(+)}\rangle.$$

The states $|\mathbf{k}'a'\rangle$ form a complete set in the space of states coupled by the interaction U, and so we can sum over the final states and use closure to remove explicit reference to them. We thus obtain the direct cross section,

$$\sigma^{dir} = \sum_{\mathbf{k}'a'}\sigma_{\mathbf{k}'a',\mathbf{k}a} \qquad (A11)$$
$$= \pi\frac{\Omega}{k}\frac{2\mu_a}{\hbar^2}\langle \psi_{\mathbf{k}a}^{(+)}|U^{\dagger}\,\delta(E - H_0)\,U|\psi_{\mathbf{k}a}^{(+)}\rangle,$$

which is the result shown in Eq. (13).

We now show that this expression is identical to the second term in Eq. (A8), which is the same as in Eq. (12). To do this we use the symbolic identity relating the outgoing-wave and principal-value Green's functions for the noninteracting Hamiltonian,

$$G_0^{(+)} = \frac{\mathcal{P}}{E - H_0} - i\pi\delta(E - H_0), \qquad (A12)$$

where $\mathcal{P}$ indicates that the principal value is to be taken when calculating integrals containing this Green's function. The operator $\mathcal{P}/(E - H_0)$ is Hermitian, and thus its expectation value in any configuration is purely real. Therefore, if we insert the above expression for $G_0^{(+)}$ in the second term of Eq. (A8), the term containing the principal-value Green's function vanishes because its matrix element has no imaginary part, and the surviving term that contains the delta function is identical to Eq. (A11).

We can put the expression for σ^{dir} of Eq. (A11) in the more familiar form of a sum over angle-integrated partial cross sections. By reinserting the complete set of final states $|\mathbf{k}'a'\rangle$ and using the definitions of Eqs. (A3)-(A5),

we obtain

$$\sigma^{dir} = \sum_{a'} \int d\hat{\mathbf{k}}' \, \frac{d\sigma_{\mathbf{k}'a', \, \mathbf{k}a}}{d\hat{\mathbf{k}}'}, \qquad (A13)$$

where the sum is over all open channels, both elastic (σ_{elas}) and otherwise (σ_{inel}). In obtaining this result we have also used the relation $\sum_{\mathbf{k}'} = \Omega/(2\pi)^3 \int d\mathbf{k}'$ to pass to the continuous variable $\mathbf{k}'$ from the discretized, box-normalized form.

Since the second term of Eq. (A8) has been identified with σ^{dir}, the first term must be σ_{cmpd} (see Eq. (1)), which is the expression shown in Eq. (10). If we write $U = V + iW$ and again use the fact that the Hermitian part V does not contribute because the matrix element is real, we get the second form, Eq. (11).

The expressions for absorption, Eqs. (10) and (11), are formally the same as for scattering in a single-channel problem. For multiple channels, these expressions include absorption from all of the coupled channels, as well as in the coupling between channels. To make this explicit, we define projection operators P_a that project onto a specific channel a such that $\sum_a P_a = 1$, and introduce the abbreviations

$$P_b|\psi_{\mathbf{k}a}^{(+)}\rangle \;=\; |\psi_{b;\mathbf{k}a}^{(+)}\rangle \qquad \text{and} \qquad (A14)$$

$$P_c W P_b \;=\; W_{cb} \qquad\qquad\qquad (A15)$$

for the projections of the state vector incident in channel a and the absorptive interaction, respectively. Thus the matrix element in Eq. (11) describing compound formation from incident channel a can be written as

$$\langle\psi_{\mathbf{k}a}^{(+)}|W|\psi_{\mathbf{k}a}^{(+)}\rangle = \sum_{cb}\langle\psi_{c;\mathbf{k}a}^{(+)}|W_{cb}|\psi_{b;\mathbf{k}a}^{(+)}\rangle. \qquad (A16)$$

There is no distinction between open and closed coupled channels, and absorption may occur from both classes. The diagonal terms $b = c$ give absorption within a channel, while the off-diagonal terms correspond to absorption during the transitions between channels. The absorption cross section obtained from this expression, supplemented by the direct interaction contribution, is nearly equivalent to the result of Hussein *et al.* in Eq. (A.11) of Ref. [20]. However, their expression lacks the off-diagonal terms, since they assumed that the channel-coupling part of the interaction was Hermitian.

The derivations of σ_{cmpd} and σ^{dir} refer to specific projections of the projectile and target spins (which are contained in the incident channel index a), and in an application these cross sections must be appropriately summed

and averaged over the projections. Charged particles may be treated by the artifice of including a large shielding radius R. In this case, the expressions for σ_{cmpd} are valid as $R \to \infty$, but those for σ^{dir} are not, since they contain the divergent elastic scattering.

Appendix B: Rare-earth optical potential

In this appendix we describe the optical potential used in the calculations for the deformed rare earth nuclei in Sec. IV B. This potential was developed for an evaluation of neutron and charged-particle cross sections in the region of samarium, europium, and gadolinium nuclei, and was determined principally from fits to neutron strength functions and total cross sections in that region [25]. The parameters are shown in Table I. The parameterization of the optical potential employed here is defined in Ref. [27], Eqs. (2)–(4). The range of applicability of this potential is 0–30 MeV. Relativistic kinematics were used in the present calculations.

TABLE I: Neutron optical model parameters for calculations on rare-earth nuclei in Sec. IV B. The asymmetry parameter η is $(N - Z)/A$, where N, Z, A are the neutron, proton, and mass numbers of the target. Energies are in MeV, and lengths in fm. E is the lab-system incident neutron energy.

Real Volume	
V_V	$50.125 - 0.2331E - (20.050 - 0.0933E)\eta$
r_V	1.25
a_V	0.65
Imaginary Volume	
W_V	$\begin{cases} 0, & E \le 8 \\ -1.357 + 0.1696E - (-0.543 + 0.0678E)\eta, & E > 8 \end{cases}$
r_V	1.25
a_V	0.65
Imaginary Surface	
W_D	$\begin{cases} 3.743 + 0.334E - (1.497 + 0.134E)\eta, & E \le 8 \\ 6.974 - 0.0697E - (2.790 - 0.0279E)\eta, & E > 8 \end{cases}$
r_D	1.25
a_D	0.58
Real Spin Orbit	
V_{SO}	8.427
r_{SO}	1.25
a_{SO}	0.65

[1] T. Kawano, P. Talou, J. E. Lynn, M. B. Chadwick, and D. G. Madland, Phys. Rev. C **80**, 024611 (2009).

[2] C. Lagrange, O. Bersillon, and D. G. Madland, Nucl. Sci. Eng. **83**, 396 (1983).

[3] ENSDF database, available at `www.nndc.bnl.gov` and mirror web sites.

[4] D. Belic *et al.*, Phys. Rev. C **65**, 035801 (2002).

[5] S. Kimura and N. Takigawa, Phys. Rev. C **66**, 024603

(2002).

[6] M. S. Hussein, Phys. Rev. C **30**, 1962 (1984).

[7] R. C. Barrett, Nucl. Phys. **51**, 27 (1964).

[8] T. Tamura, Rev. Mod. Phys. **37**, 679 (1965).

[9] E. S. Sukhovitskii, O. Iwamoto, S. Chiba, and T. Fukahori, J. Nucl. Sci. and Tech. **37**, 120 (2000).

[10] J. E. Escher and F. S. Dietrich, Phys. Rev. C **81**, 024612 (2010).

[11] J. Raynal, *computer code* ECIS06, unpublished (2006).

[12] I. J. Thompson, Comp. Phys. Reports **7**, 167 (1988).

[13] I. J. Thompson, FRESCO*, ver. FRXY.5j*, unpublished (2005).

[14] T. Kawano, *computer code CoH₃*, unpublished (2010).

[15] A. Bohr and B. Mottelson, *Nuclear Structure, Vol. II* (Benjamin, New York, 1975).

[16] C. E. Porter, Phys. Rev. **100**, 935 (1955).

[17] J. Cugnon, Nucl. Phys. **A263**, 47 (1976).

[18] L. I. Schiff, *Quantum Mechanics, Third Edition,* Ch. 5, Sec. 20 (McGraw-Hill, New York, 1968).

[19] M. S. Hussein, Ann. Phys. (N.Y.) **175**, 197 (1987).

[20] M. S. Hussein, R. A. Rego, and C. A. Bertulani, Phys. Reports **201**, 279 (1991).

[21] A. R. Edmonds, *Angular Momentum in Quantum Mechanics, 2nd edition* (Princeton University Press, Princeton, 1960).

[22] A. Bohr and B. Mottelson, *Nuclear Structure, Vol. I* (Benjamin, New York, 1969).

[23] S. Drozdov, Soviet Physics (JETP) **1**, 588, 591 (1955).

[24] D. M. Chase, L. Wilets, and A. R. Edmonds, Phys. Rev. **110**, 1080 (1958).

[25] R. D. Hoffman, K. Kelley, F. S. Dietrich, R. Bauer, and M. Mustafa, Tech. Rep. UCRL-TR-211558, Lawrence Livermore National Laboratory, Livermore, CA (2005).

[26] D. L. Hendrie, N. K. Glendenning, B. G. Harvey, O. N. Jarvis, H. H. Duhm, J. Saudinos, and J. Mahoney, Phys. Lett. **26B**, 127 (1968).

[27] A. J. Koning and J.-P. Delaroche, Nucl. Phys. **A713**, 231 (2003).

[28] H. Rebel, G. W. Schweimer, J. Specht, G. Schatz, R. Löhken, D. Habs, G. Hauser, and H. Klewe-Nebenius, Phys. Rev. Lett. **26**, 1190 (1971).

[29] R. W. Finlay, W. P. Abfalterer, G. Fink, E. Montei, T. Adami, P. W. Lisowski, G. L. Morgan, and R. C. Haight, Phys. Rev. C **47**, 237 (1993).

[30] W. P. Abfalterer, F. B. Bateman, F. S. Dietrich, R. W. Finlay, R. C. Haight, and G. L. Morgan, Phys. Rev. C **63**, 044608 (2001).

[31] W. P. Poenitz, J. F. Whalen, and A. B. Smith, Nucl. Sci. Eng. **78**, 333 (1981).

[32] B. Margolis and E. S. Troubetzkoy, Phys. Rev. **106**, 105 (1957).

[33] R. G. Newton, Am. J. Phys. **44**, 639 (1976).

[34] H. C. van de Hulst, Physica **15**, 740 (1949).